Determination of hip-joint loading patterns of living and extinct mammals using an inverse Wolff's law approach

P. Christen, K. Ito, F. Galis, B. van Rietbergen

Biomech Model Mechanobiol (2015) 14:427–432
DOI 10.1007/s10237-014-0602-8

SHORT COMMUNICATION

Determination of hip-joint loading patterns of living and extinct mammals using an inverse Wolff's law approach

Patrik Christen · Keita Ito · Frietson Galis · Bert van Rietbergen

Received: 5 March 2014 / Accepted: 9 June 2014 / Published online: 21 June 2014

Abstract It is well known that bone adapts its microstructure in response to loading. Based on this form-follows-function relationship, we previously developed a reverse approach to derive joint loads from bone microstructure as acquired with micro-computed tomography. Here, we challenge this approach by calculating hip-joint loading patterns for human and dog, two species exhibiting different locomotion, and comparing them to in vivo measurements. As a proof of concept to use the approach also for extinct taxa, we applied it to a cave lion fossil bone. Calculations were in close agreement with in vivo measurements during walking for extant species, showing distinguished patterns for bipedalism and quadrupedalism. The cave lion calculations clearly revealed its quadrupedal locomotion and suggested a more diverse behaviour compared to the dog, which is in agreement with extant felids. This indicates that our novel approach is potentially useful for making inferences about locomotion in living as well as extinct mammals and to study evolutionary joint development.

P. Christen · K. Ito · B. van Rietbergen (✉)
Orthopaedic Biomechanics, Department of Biomedical Engineering, Eindhoven University of Technology, P.O. Box 513, 5600 MB Eindhoven, The Netherlands
e-mail: b.v.rietbergen@tue.nl

F. Galis
Naturalis Biodiversity Center, Darwinweg 2, 2333 CR Leiden, The Netherlands

Present Address:
P. Christen
Department of Zoology, University of Oxford, South Parks Road, Oxford OX1 3PS, UK

Keywords Bone form–function relationship · Hip-joint loading patterns · Bone/fossil microstructure · Locomotion · Micro-computed tomography · Micro-finite element modelling.

1 Introduction

Bone can adapt its microstructure by means of a life-long process in which osteoblasts add bone tissue at locations of high mechanical loading, and osteoclasts remove it at locations of low mechanical loading. Osteocytes in the bone are capable of sensing local tissue loading and are thus considered to trigger bone adaptation according to mechanical loading. This process strives to create a state where all bone tissue is loaded as uniformly as possible in order to avoid peak loads and unnecessary weight (Barak et al. 2011; Lambers et al. 2011; Pontzer et al. 2006; Roux 1881; Schulte et al. 2013; Sugiyama et al. 2012, 2010; Wolff 1892). The form–function relationship due to bone adaptation implies that it might be possible as well to reversely derive hip-joint loading patterns from the femoral head microstructure by finding a set of joint forces that produce such a state of uniform tissue loading. In an earlier study, we developed a computational algorithm based on this principle (Christen et al. 2012). In the present study, we apply this algorithm reconstructing the elaborate loading patterns at the hip joint for human and dog, two species exhibiting different locomotion. Results are compared to direct in vivo force measurements using instrumented implants, as reported in the literature (Bergmann et al. 2001, 1993, 1984; Page et al. 1993). Considering the potential to reconstruct joint loads and thus infer locomotion of extinct animals based on their fossil remains, as a proof of concept, the algorithm is also applied to predict the loading pattern for an extinct cave lion based on microstructure

measurement obtained from a fossil femur. Since both, cave lion and dog, are quadrupeds, their loading patterns are expected to be similar but different from human bipedalism.

2 Materials and methods

2.1 Human and dog samples

Two human and one canine (flat-coated retriever) cadaver femoral heads were used. Human samples were from a healthy (T-score: −0.5) and an osteoporotic (T-score: −4.0) donor of similar age (82 and 89 years), weight (63 and 57 kg), and height (1.60 and 1.61 m) (Van Rietbergen et al. 2003). Trabecular bone volume fractions measured for a cubic region at the centre of the femoral head were 0.50 for the healthy human, 0.28 for the osteoporotic human, and 0.44 for the dog.

2.2 Cave lion fossil

To apply the approach to extinct taxa, a Pleistocene *Panthera leo spelaea* fossil femur (RGM St. 369296) from the collection of the Naturalis Biodiversity Center in Leiden, the Netherlands, was used. The specimen was found in the Brown Ridge area, 80 km to the west of the Dutch shore near IJmuiden in the North Sea (52°25′ N., 3°00′ O.) (Gross 1992).

2.3 Body weights

The healthy and osteoporotic human donors had a weight of 63 and 57 kg, respectively (Van Rietbergen et al. 2003). For the canine, a value of 30 kg was used and for the cave lion, an estimate of 250 kg. The size of the cave lion femur is comparable to the upper half of the size variation in modern lions as measured earlier (Gross 1992). Based on this, we chose the cave lion body weight in accordance with the *Panthera leo* body weight range (Walker and Nowak 1991). These body weights were finally used to report the calculated loading in per cent body weight.

2.4 Image acquisition and segmentation

Bone microstructure of the femoral heads was assessed using micro-computed tomography (micro-CT) (Fig. 1). Human bones were imaged at an isotropic resolution of 80 μm in a previous study using a prototype of a micro-CT device (μCT 80 prototype, Scanco Medical AG, Switzerland) (Van Rietbergen et al. 2003). Segmentation was performed using a fixed global threshold based on the image histograms. The canine sample was scanned in the present study at an isotropic resolution of 37 μm using micro-CT (μCT 80, Scanco Medical AG, Switzerland) and the cave lion fossil at 82 μm using high-resolution peripheral quantitative CT (XtremeCT, Scanco Medical AG, Switzerland). Images of both species were Gaussian filtered (dog: sigma = 0.8, support = 1 voxel; lion: sigma = 1.0, support = 3 voxels) to remove noise and segmented using a fixed global threshold (dog: 220/1,000; lion: 180/1,000 of the maximum greyscale value) to distinguish bone from marrow. In all cases, filtering and segmenting parameters were chosen in such a way to match the original greyscale image as close as possible. Since fossil bone imaging is challenging due to possible in-filling of sediments, a comparison of the original and segmented image is provided for the cave lion (Fig. 2). Image processing language (IPL, Scanco Medical AG, Switzerland) was used for all image processing.

2.5 Micro-FE modelling and load estimation algorithm

Based on the micro-CT images, hip-joint forces were calculated using a recently developed load estimation algorithm (Christen et al. 2012). This approach is based on the assumption that bone strives for a uniform tissue loading distribution. In a first step, micro-finite element (micro-FE) models of the femoral heads were generated based on the micro-CT images by directly transforming image voxels into regular hexahedral finite elements (Van Rietbergen et al. 1995). Only the head and neck region were modelled, resulting in FE models with a large number of bone elements in the healthy human (39,875,119 elements), osteoporotic human (26,294,495 elements), dog (38,603,304 elements), and cave lion (43,194,155 elements). Micro-FE analyses were then performed to calculate the actual tissue loading for a set of unit loads using the Scanco FE-solver (IPLFE, Scanco Medical AG, Switzerland). Unit loads were evenly distributed over the contact area of the femoral head and applied as distributed forces (with a resulting initial total force of $F_{\text{unit}} = 1$ kN) following a cosine function of the polar angle with respect to the femoral head centre and perpendicular to the articular surface, whereas the distal ends of the femurs were fully constrained. This led to a total of 29 load cases in the healthy human, 27 in the osteoporotic human, 33 in the dog, and 34 in the cave lion. The applied forces should well cover the physiologically possible range of loading since forces in the joint act normal to the surface, assuming non-frictional contact, and within the articulating surface. Tissue loading was quantified as strain energy density (SED), U, for each unit load, i, and element, x, of the micro-FE models. Tissue properties were modelled linear elastic with a Young's modulus of 10 GPa and a Poison's ratio of 0.3 for all species (Pressel et al. 2005; Van Rietbergen et al. 1995; Zysset et al. 1999). Equal bone tissue material properties in the femur across species are assumed based on a study showing that bone material properties of long bones do not vary much within mammals and that the first material properties

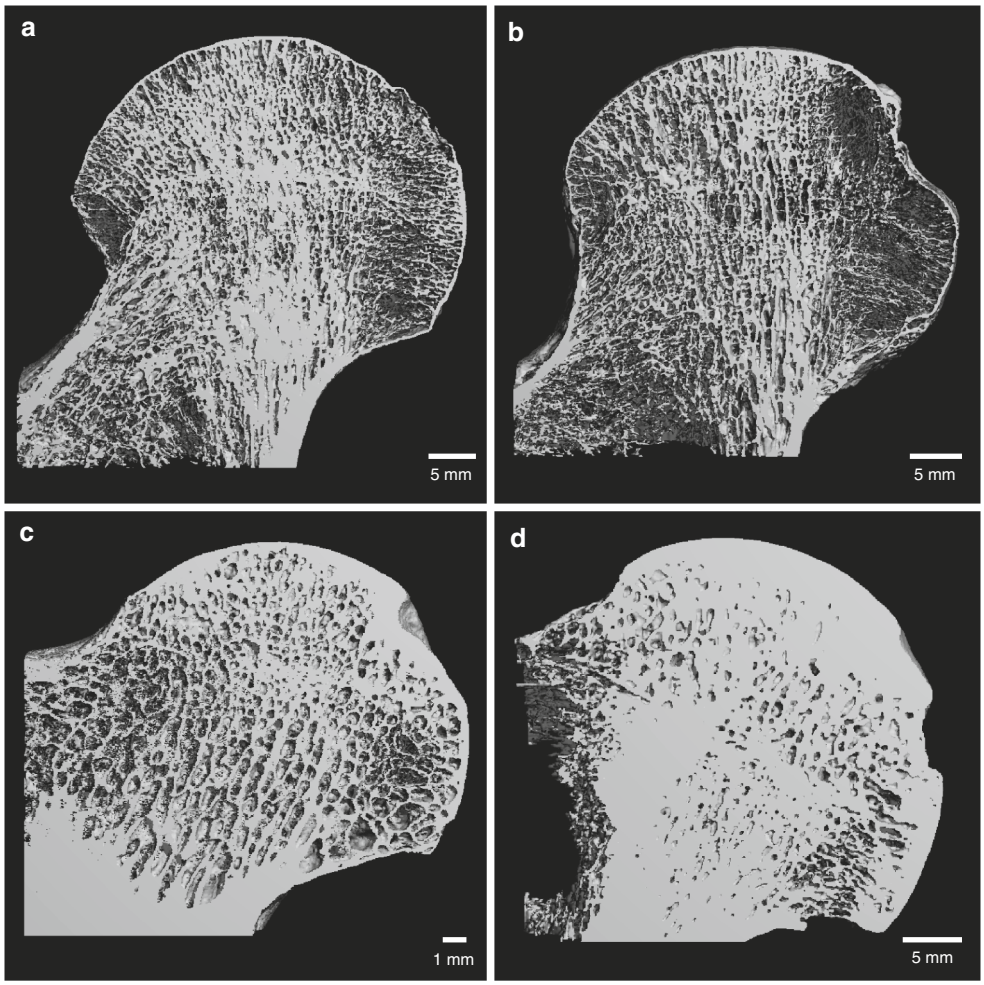

Fig. 1 Bone microstructures as acquired by micro-computed tomography for human, healthy (**a**) and osteoporotic (**b**), dog (**c**), and cave lion (**d**) femoral heads

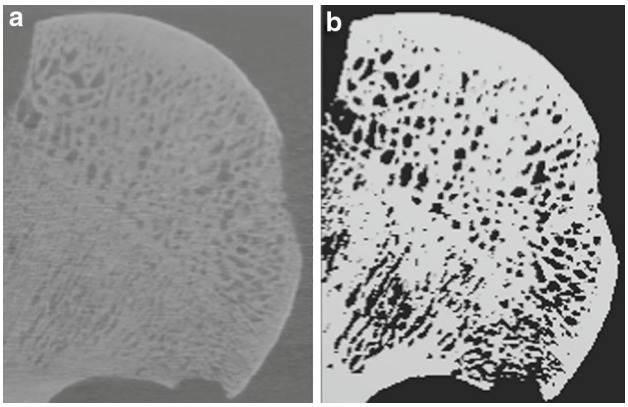

Fig. 2 Original micro-computed tomography scan (**a**) and the segmented image (**b**) of the cave lion fossil femoral head

for long bones were conserved throughout evolution over the time course of 475 million years (Erickson et al. 2002). In a second step, the hip-joint forces were calculated by scaling the set of n predefined unit loads until the summed resultant SED of each load case, $U_i(x)$, reached the most uniform SED distribution (Fig. 3). This can be formulated as an optimisation problem finding the scaling factors, s_i, minimising the residual, $r(s_i)$, over the bone volume, V:

$$\min_{s_i} r(s_i) = \int \left[\sum_{i=1}^{n} [s_i U_i(x)] - k \right]^2 \mathrm{d}V$$

where k is a physiological target value for the local SED, which was set to 0.02 MPa (Mullender and Huiskes 1995). Non-negative least square optimisation (Lawson and Hanson 1974) is then used to calculate the scaling factors. Assuming that all unit loads act equally long, the final force magnitude, α_i, is calculated by scaling the initial unit force, F_{unit}, as follows: $\alpha_i = \sqrt{s_i} F_{\mathrm{unit}}$.

3 Results

The algorithm calculated peak forces of up to 458 % body weight (BW), 237 % BW and 214 % BW, for the healthy

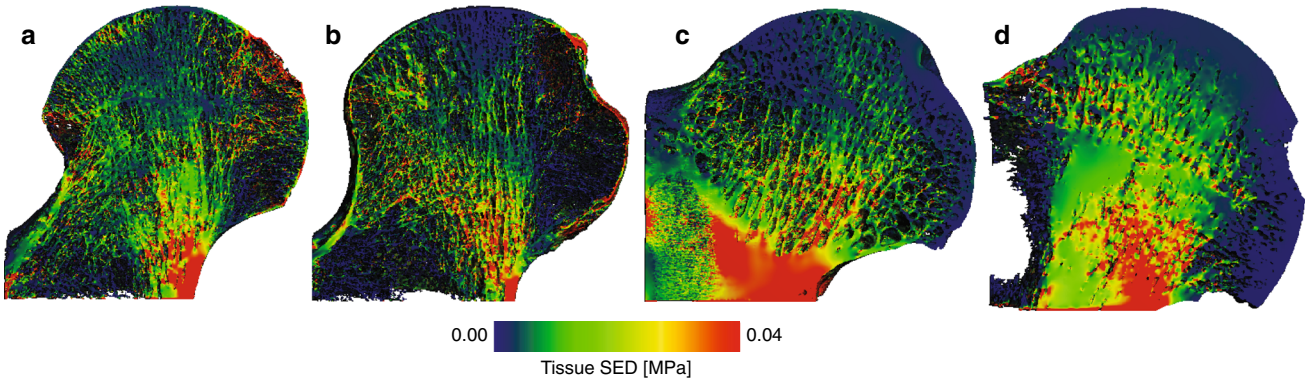

Fig. 3 Tissue loading distribution at the microscopic level represented as strain energy density (SED) for human, healthy (**a**) and osteoporotic (**b**), dog (**c**), and cave lion (**d**) femoral heads. Distributions are determined based on the calculated loading and thus represent the best possible uniform distributions as found by the optimisation procedure

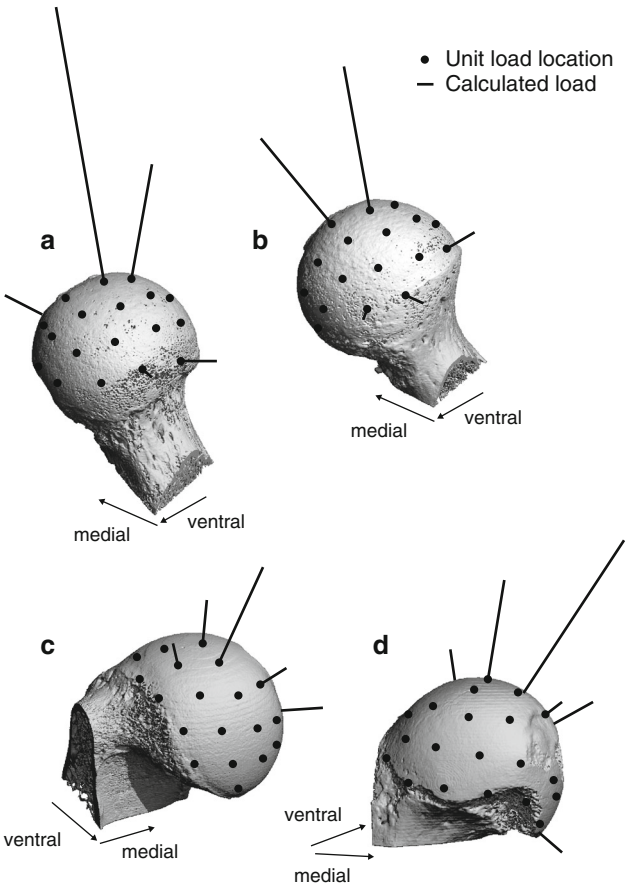

Fig. 4 Calculated hip-joint loading patterns for human, healthy (**a**) and osteoporotic (**b**), dog (**c**), and cave lion (**d**)

human, osteoporotic human, and dog, respectively (Fig. 4a–c). For humans, the main forces (of largest magnitude) were calculated for the superior end of the femoral head, whereas for the dog, these forces also started superior of the femoral head but spread medially (Fig. 4a–c). Calculated human and canine loading patterns compare favourably with in vivo measurements during walking (Bergmann et al. 2001, 1993, 1984; Page et al. 1993). Only some small forces approximately ten times smaller than the main forces calculated for the lateral and medial rim were not in agreement in the human case (Fig. 4a, b). Since in vivo measurements only provide the resultant force, they may not be able to account for such forces. For the cave lion, a peak force of 196 % BW was found and calculated main forces started superior of the femoral head and spread medially (Fig. 4d).

4 Discussion

Calculated peak forces for human and dog compare well to in vivo hip-joint force measurements from the literature that showed peak forces during stance phase of normal walking of 211–410 % BW in humans (Bergmann et al. 2001, 1993, 1984) and approximately 165 % BW in dogs (Page et al. 1993). At least in humans, these values depend on the walking speed as shown by increasing values from 280 % BW at 1 km h^{-1} to 480 % BW at 5 km h^{-1}, and 550 % BW when jogging (Bergmann et al. 1993). Peak forces measured during normal walking are slightly below our estimates, likely because our approach provides estimates of the prevalent loading history also including larger forces such as during faster walking or jogging. The force magnitude calculated for the healthy human donor was almost twice as high as that calculated for the osteoporotic donor. This difference is in good agreement with the difference in bone density, which was also almost twice as high in the healthy donor, suggesting a near linear relationship between femoral bone density and loading. It should be noted, however, that no history of these donors was available. It is possible, for example, that the osteoporotic femur was obtained from a wheelchair or bedridden donor, in which case the predictions for the osteoporotic femur could be overestimating the actual loading if the bone is no longer adapted to its mechanical environment.

Peak forces for dog and cave lion are in the same range. Also, the calculated loading patterns, including forces spread

medially, are in agreement. For both, dog and cave lion, calculated main forces were rather spread over the femoral head surface, typical for quadrupedalism (Bergmann et al. 1984), whereas in human, these forces were concentrated at the superior end of the femoral head (Fig. 4). These results indicate that our calculated hip-joint forces allow inferring the major locomotor modes bipedalism and quadrupedalism and can provide quantitative information about the magnitude of forces the bones were subjected to. The estimated hip-joint forces could then be used in biomechanical models of animal locomotion (Hutchinson and Gatesy 2006), constraining joint range of motion and providing force magnitudes that would be especially useful in cases where these model parameters are not exactly known such as in extinct animals.

Calculated loading patterns of dog and cave lion reveal differences in locomotor behaviour of the two species. Estimated hip-joint forces for the cave lion are less uniform because they cover a wider range of magnitudes and the peak force seems more distinguished from the smaller forces (Fig. 4c, d). This suggests a more diverse locomotor behaviour of the cave lion, which could be related to preying activities such as jumping. In general, felids exhibit a wider range of femoral postures and a more flexible spine than canines improving their jumping and agility performance (Jenkins and Camazine 1977). The diverse loading pattern calculated for the cave lion is thus in agreement with the behaviour of extant felids. This indicates the potential of the present approach to distinguish and infer species-specific locomotion.

Although revealing promising results, there are limitations to our study that need to be discussed and require further consideration in future studies. First, we used a small sample size. However, animals with different locomotion behaviour were chosen to get a first impression how well the approach works across species, and our results encourage conducting more studies to validate the approach for different species and joints. This would also allow rigorous validation of the method for long bones, extending the earlier validation for mice vertebrae (Christen et al. 2012) and cubic bone microstructures (Christen et al. 2013a). Second, the sensitivity of the load estimation algorithm with respect to the image resolution, location, and number of predefined unit loads was not yet thoroughly investigated. The effect of image resolution on the accuracy of micro-FE results, however, has been addressed in several earlier studies, and these studies found that for high-density bone in the femoral head, a resolution of 80 μm is adequate (Bevill and Keaveny 2009; Ulrich et al. 1998; Van Rietbergen et al. 1995). To further investigate this, we recently performed a pilot study using cubic bone microstructures. In that study, we found that estimates of the normal forces differed by less than 20 % when changing the resolution from 20 to 80 μm, suggesting that the approach is not very sensitive to the actual image resolution in that range. Related to this, the question whether the algorithm is sensitive enough to detect subtle differences in loading patterns needed for answering evolutionary questions between extinct species remains to be investigated. Third, segmenting fossil bones is not straightforward due to possible artefacts from partially fossilised specimens or post-depositional infilling of the inter-trabecular space. The uncommonly high trabecular bone volume fraction of the cave lion fossil of 0.71 in our study indicates such an artefact on first sight. However, segmentation thresholds were defined according visual check of the greyscale images, and only one phase of mineral seemed to be present allowing proper segmentation (Fig. 2). Fourth, small forces at the lateral and medial rim were calculated but not measured in vivo in humans (Fig. 4a, b). Such forces are most likely not possible to measure with instrumented hip implants since there is no rim that could limit the motion in the hip joint and there is also no incongruence between femoral head and acetabulum distributing central forces to the rim. And fifth, mechanical forces are not the only determinate of bone microstructure, complicating the structure–function relationship. Bone is a dynamic tissue storing calcium and phosphorus and responding to metabolic and nutritional changes. It is therefore evident that bone microstructure is not only adapted to local loading conditions but is also determined by non-targeted bone remodelling to fulfil metabolic demands such as maintaining calcium homoeostasis (Burr 2002). This also explains why the tissue loading is not perfectly homogeneous as found in the present study (Fig. 3). Nevertheless, we know most bone formation takes place at high-load locations and most resorption at low-load locations (Schulte et al. 2013), and this seems to be enough for our algorithm to reveal a reasonable loading history as demonstrated in the present and also earlier studies (Christen et al. 2013b, 2012).

The main novelty of this study is that it indicates the potential of deriving hip-joint loading patterns from present and fossil bone microstructure. Deciphering this hidden message within bone could be particularly useful to make inferences about locomotion in cases where direct measurements are not possible, but bone structures are available. Although the present study provides a first proof of concept for the latter, it is clear that this approach relies on an accurate segmentation of the bone structure from fossil bones, which will need further investigation. In broader perspective, the presented approach could also be useful to study evolutionary aspects of joint development and loading in mammals. But first, the outlined limitations with respect to validation, sensitivity, and fossil image segmentation need to be addressed in future research.

Acknowledgments We thank Reinier van Zelst and Steven D. van der Mije from Naturalis Biodiversity Center for providing a cave lion fossil, Claudia F. Wolschrijn from Utrecht University for providing a

dog femur, Ralph Müller from ETH Zurich for support through the VPHOP WP5 group, Joost J.A. de Jong for helping scanning the cave lion fossil, and Joop P.W. van den Bergh for providing the XtremeCT facility at Maastricht University. Funding from the European Union for the osteoporotic virtual physiological human project (VPHOP FP7-ICT2008-223865) is gratefully acknowledged.

References

Barak MM, Lieberman DE, Hublin JJ (2011) A Wolff in sheep's clothing: trabecular bone adaptation in response to changes in joint loading orientation. Bone 49:1141–1151. doi:10.1016/J.Bone.08.020

Bergmann G, Siraky J, Rohlmann A, Koelbel R (1984) A comparison of hip-joint forces in sheep, dog and man. J Biomech 17:907. doi:10.1016/0021-9290(84)90004-6

Bergmann G, Graichen F, Rohlmann A (1993) Hip-joint loading during walking and running, measured in 2 patients. J Biomech 26:969–990. doi:10.1016/0021-9290(93)90058-M

Bergmann G, Deuretzbacher G, Heller M, Graichen F, Rohlmann A, Strauss J, Duda GN (2001) Hip contact forces and gait patterns from routine activities. J Biomech 34:859–871. doi:10.1016/S0021-9290(01)00040-9

Bevill G, Keaveny TM (2009) Trabecular bone strength predictions using finite element analysis of micro-scale images at limited spatial resolution. Bone 44:579–584. doi:10.1016/j.bone.2008.11.020

Burr DB (2002) Targeted and nontargeted remodeling. Bone 30:2–4. doi:10.1016/S8756-3282(01)00619-6

Christen P, van Rietbergen B, Lambers FM, Muller R, Ito K (2012) Bone morphology allows estimation of loading history in a murine model of bone adaptation. Biomech Model Mech 11:483–492. doi:10.1007/S10237-011-0327-X

Christen P, Ito K, dos Santos AA, Muller R, van Rietbergen B (2013a) Validation of a bone loading estimation algorithm for patient-specific bone remodelling simulations. J Biomech 46:941–948. doi:10.1016/J.Jbiomech.2012.12.012

Christen P, Ito K, Knippels I, Muller R, van Lenthe GH, van Rietbergen B (2013b) Subject-specific bone loading estimation in the human distal radius. J Biomech 46:759–766. doi:10.1016/J.Jbiomech.2012.11.016

Erickson GM, Catanese J, Keaveny TM (2002) Evolution of the biomechanical material properties of the femur. Anat Rec 268:115–124. doi:10.1002/Ar.10145

Gross C (1992) Das Skelett des Höhlenlöwen (Panthera leo spelaea Goldfuss, 1810) aus Siegsdorf/Ldkr. Traunstein im Vergleich mit anderen Funden aus Deutschland und den Niederlanden. PhD Thesis, Tierärztliche Fakultät der Maximilians-Universität, München

Hutchinson JR, Gatesy SM (2006) Dinosaur locomotion—beyond the bones. Nature 440:292–294. doi:10.1038/440292a

Jenkins FA, Camazine SM (1977) Hip structure and locomotion in ambulatory and cursorial carnivores. J Zool 181:351–370

Lambers FM, Schulte FA, Kuhn G, Webster DJ, Muller R (2011) Mouse tail vertebrae adapt to cyclic mechanical loading by increasing bone formation rate and decreasing bone resorption rate as shown by time-lapsed in vivo imaging of dynamic bone morphometry. Bone 49:1340–1350. doi:10.1016/J.Bone.2011.08.035

Lawson CL, Hanson RJ (1974) Solving least squares problems. Prentice-Hall International, Englewood Cliffs

Mullender MG, Huiskes R (1995) Proposal for the regulatory mechanism of Wolff's law. J Orthopaed Res 13:503–512. doi:10.1002/Jor.1100130405

Page AE, Allan C, Jasty M, Harrigan TP, Bragdon CR, Harris WH (1993) Determination of loading parameters in the canine hip in vivo. J Biomech 26:571–579. doi:10.1016/0021-9290(93)90018-A

Pontzer H, Lieberman DE, Momin E, Devlin MJ, Polk JD, Hallgrimsson B, Cooper DML (2006) Trabecular bone in the bird knee responds with high sensitivity to changes in load orientation. J Exp Biol 209:57–65. doi:10.1242/Jeb.01971

Pressel T, Bouguecha A, Vogt U, Meyer-Lindenberg A, Behrens BA, Nolte I, Windhagen H (2005) Mechanical properties of femoral trabecular bone in dogs. Biomed Eng Online 4:17. doi:10.1186/1475-925X-4-17

Roux W (1881) Der Kampf der Theile im Organismus. Ein Beitrag zur Vervollständigung der mechanischen Zweckmässigkeitslehre. Verlag von Wilhelm Engelmann, Leipzig

Schulte FA, Ruffoni D, Lambers FM, Christen D, Webster DJ, Kuhn G, Muller R (2013) Local mechanical stimuli regulate bone formation and resorption in mice at the tissue level. Plos One 8. doi:10.1371/journal.pone.0062172

Sugiyama T, Meakin LB, Browne WJ, Galea GL, Price JS, Lanyon LE (2012) Bones' adaptive response to mechanical loading is essentially linear between the low strains associated with disuse and the high strains associated with the lamellar/woven bone transition. J Bone Miner Res 27:1784–1793. doi:10.1002/Jbmr.1599

Sugiyama T, Price JS, Lanyon LE (2010) Functional adaptation to mechanical loading in both cortical and cancellous bone is controlled locally and is confined to the loaded bones. Bone 46:314–321. doi:10.1016/J.Bone.2009.08.054

Ulrich D, van Rietbergen B, Weinans H, Ruegsegger P (1998) Finite element analysis of trabecular bone structure: a comparison of image-based meshing techniques. J Biomech 31:1187–1192

Van Rietbergen B, Huiskes R, Eckstein F, Ruegsegger P (2003) Trabecular bone tissue strains in the healthy and osteoporotic human femur. J Bone Miner Res 18:1781–1788. doi:10.1359/Jbmr.2003.18.10.1781

Van Rietbergen B, Weinans H, Huiskes R, Odgaard A (1995) A new method to determine trabecular bone elastic properties and loading using micromechanical finite-element models. J Biomech 28:69–81

Walker EP, Nowak RM (1991) Walker's mammals of the world, 5th edn. Johns Hopkins University Press, Baltimore

Wolff J (1892) Das Gesetz der Transformation der Knochen. Verlag von August Hirschwald, Berlin

Zysset PK, Guo XE, Hoffler CE, Moore KE, Goldstein SA (1999) Elastic modulus and hardness of cortical and trabecular bone lamellae measured by nanoindentation in the human femur. J Biomech 32:1005–1012. doi:10.1016/S0021-9290(99)00111-6